HHS Public Access

Author manuscript

J Magn Reson Imaging. Author manuscript; available in PMC 2020 February 01.

Published in final edited form as:

J Magn Reson Imaging. 2019 February ; 49(2): 534–545. doi:10.1002/jmri.26206.

Uteroplacental and Fetal 4D Flow MRI in the Pregnant Rhesus Macaque

Jacob A Macdonald, MS[1], **Philip A Corrado, BS**[1], **Sydney M Nguyen, BS**[2], **Kevin M Johnson, PhD**[1], **Christopher J Francois, MD**[3], **Ronald R Magness, PhD**[4], **Dinesh M Shah, MD**[5], **Thaddeus G Golos, PhD**[2,6], and **Oliver Wieben, PhD**[1,3]

[1]Department of Medical Physics, University of Wisconsin – Madison, Madison, WI

[2]Wisconsin National Primate Center, University of Wisconsin – Madison, Madison, WI

[3]Department of Radiology, University of Wisconsin – Madison, Madison, WI

[4]Department of Obstetrics & Gynecology, University of South Florida, Tampa, FL

[5]Department of Obstetrics & Gynecology, University of Wisconsin – Madison, Madison, WI

[6]Department of Comparative Biosciences, University of Wisconsin – Madison, Madison, WI

Abstract

BACKGROUND—Pregnancy complications are often associated with poor uteroplacental vascular adaptation and standard diagnostics are unable to reliably quantify flow in all uteroplacental vessels and have poor sensitivity early in gestation.

PURPOSE—To investigate the feasibility of using 4D flow MRI to assess total uteroplacental blood flow in pregnant rhesus macaques as a precursor to human studies.

STUDY TYPE—Retrospective feasibility study

ANIMAL MODEL—Fifteen healthy, pregnant rhesus macaques ranging from 1st trimester to 3rd trimester of gestation.

FIELD STRENGTH/SEQUENCE—Abdominal 4D flow MRI was performed on a 3.0T scanner with a radially-undersampled phase contrast (PC) sequence. Reference ferumoxytol-enhanced angiograms were acquired with a 3D ultrashort echo time sequence with a center-out radial trajectory.

ASSESSMENT—Repeatability of flow measurements was assessed with scans performed same-day and on consecutive days in the uterine arteries and ovarian veins. In-flow was compared against out-flow in the uterus, umbilical cord, and fetal heart with a conservation of mass analysis. Conspicuity of uteroplacental vessels was qualitatively compared between PC angiograms derived from 4D flow data and ferumoxytol-enhanced angiograms.

STATISTICAL TESTS—Bland-Altman analysis was used to quantify same-day and consecutive-day repeatability.

Corresponding Author: Oliver Wieben PhD, Address: 1111 Highland Avenue, Room 1005, Madison, WI 53705. Telephone: 608-263-0793. owieben@wisc.edu.

RESULTS—Same-day flow measurements showed an average difference between scans of 13% in both the uterine arteries and ovarian veins, while consecutive day measurements showed average differences of 22% and 24% respectively. Comparisons of in-flow and out-flow showed average differences of 15% in the uterus, 8% in fetal heart, and 15% in the umbilical cord. PC angiograms showed similar depiction of main uteroplacental vessels as high-resolution, ferumoxytol-enhanced angiograms.

DATA CONCLUSION—4D flow MRI could be used in the rhesus macaque for repeatable flow measurements in the uteroplacental and fetal vasculature, setting the stage for future human studies.

Keywords

4D flow; uterine blood flow; fetal blood flow; placenta; pregnancy

INTRODUCTION

Many pregnancy complications are associated with poor uteroplacental vascular adaptation to placental and fetal growth. Compromised uteroplacental blood flow and placental perfusion has been linked to fetal growth restriction (FGR) [1,2], preeclampsia, preterm birth, and stillbirth [3–5]. Non-invasive assessment of uteroplacental blood flow and function could play an important role in detecting insufficient blood flow to the placenta and guide decision making to reduce adverse effects, particularly if used in early stages of pregnancy before clinical manifestation of adverse pathophysiology [6]. For example, there is strong clinical evidence that low-dose aspirin can reduce the risk of FGR and preeclampsia in women with reduced blood flow [7], and intensified monitoring of these pregnancies can allow for appropriately timed delivery.

As shown in Figure 1, most of the maternal oxygenated blood enters the placenta through the left and right uterine arteries (UtA) with additional contributions through the left and right uterine branches of the ovarian arteries (ovarian stem arteries (OSA)) [8,9]. Hence, comprehensive characterization of total uteroplacental blood flow requires measurements in these arteries or their corresponding veins. On the fetal side, two umbilical arteries carry deoxygenated, nutrient-depleted blood from the fetus to the placenta, and oxygenated, nutrient-rich blood is returned from the placenta to the growing fetus through the umbilical vein.

Hemodynamics in the UtAs, umbilical vessels, and fetal aorta are routinely assessed with Doppler ultrasound (US). US offers high temporal resolution and is widely availability in prenatal care. Abnormal uteroplacental flow is detected through velocity waveform analysis by grading of the presence of a pre-diastolic notch and quantitative measures of the resistive index (RI) and pulsatility index (PI) [10,11]. Measures of vascular resistance in the fetal umbilical arteries are used to approximate fetal-placental resistance in high-risk pregnancies [12]. PI measurements in the fetal aorta can also be used to identify potential hypoxia or FGR [13].

However, there are inherent limitations with US. Doppler US cannot directly measure flow, but instead estimates these measurements by fitting acquired velocity information to pre-established vascular velocity profiles. Inaccuracies in these models can introduce systematic errors into blood flow estimates [14] and hence, vessels with complex geometry and pulsatile flow such as the torturous UtAs and OSAs are ill-suited for Doppler flow measurements, and complementary measures such as RI and PI are used instead. RI and PI, however, have limited prognostic abilities for preeclampsia and FGR, with low sensitivity early in gestation [15–17]. In addition, Doppler US is typically unable to visualize contributions from the OSAs, and thus cannot determine total uteroplacental blood flow in humans. Finally, due to beam attenuation in the body, image quality while assessing the umbilical arteries and fetal vessels depends on the positioning of the fetus and transducer placement. These limitations are further exacerbated in obese patients, a significant subject population in North America.

MRI is arguably well-suited to probe placental function and health during pregnancy as it can potentially quantify uteroplacental flow, perfusion [18], and tissue oxygenation [19]. Currently, MRI is not used for screening maternal or fetal health during pregnancy and is limited to surgical indications, such as suspected appendicitis [20], due to higher costs and the lack of definitive safety studies [21,22]. With validated protocols and dedicated safety studies, however, MRI flow analysis could improve early identification of pregnancy complications and enable and monitor therapeutic interventions in high-risk populations.

Previous studies have attempted flow measurements in uteroplacental vessels with 2D phase contrast (PC) MRI [23]. One such 2D PC feasibility study aimed to measure total uteroplacental blood flow but encountered difficulties in prescribing scan planes orthogonal to the small and torturous UtAs and OSAs from MR angiograms [24]. Another compared 2D PC and Doppler US flow estimates in the UtAs with good agreement in early 3rd trimester when the uteroplacental vessels had remodeled and dilated [25]. However, the ovarian branches were not included and detection of abnormalities at this stage in pregnancy are too late for optimal therapeutic intervention.

4D flow MRI [26] has shown potential for assessing vascular anatomy and hemodynamics in complex vascular territories, such as congenital heart disease [27] and intracranial arteriovenous malformations [28]. The inherently provided PC MR Angiograms (PC MRA) can be used to visualize the vascular anatomy in 3D and orient measurement planes orthogonal to vessels of interest in post-processing rather than during scanning. Capturing the UtAs and OSAs in a single scan requires a large imaging volume and, therefore, long acquisition times with traditional Cartesian encoding. This is problematic because of the possibility of motion artifacts from maternal breathing, fetal cardiac motion, fetal movements, and the pulsatility of the fetal and maternal cardiovascular systems. While maternal breathing and cardiac pulsatility can be mitigated through respiratory and cardiac gating, fetal motion and fetal cardiac pulsatility are challenging to control.

Herein we propose the use of Phase Contrast Vastly-undersampled Isotropic-voxel PRojection imaging (PC VIPR), a 4D flow method based on 3D radial undersampling, to overcome these obstacles in clinically feasible scan times [29,30]. The undersampled radial

trajectory allows for large volumetric coverage with high, isotropic spatial resolution. In the context of pregnancy, this permits abdominal imaging encompassing the maternal great vessels, uteroplacental vessels, placenta, and fetus in a single acquisition. Both arterial and venous flow can be measured to characterize blood supply and return pathways. The inherent oversampling of the center of k-space with a radial trajectory also provides an increased robustness to motion [31] and has been validated in regions affected by respiratory motion including cardiac, liver, and renal artery studies [32–34].

The goal of this study was to assess the feasibility and repeatability of flow measurements in the uteroplacental and fetal vasculature from a single PC VIPR acquisition, laying the groundwork for studies in human subjects. A rhesus macaque model was chosen as it allowed for scans early in pregnancy, multi-day repeatability assessment, and the use of an iron-based contrast agent for reference angiograms. The rhesus macaque features a villous organization of the placenta, extravillous trophoblast invasion with resulting remodeling of the decidual spiral arteries, and a first trimester decidual leukocyte population very similar to humans [35,36]. We hypothesize PC VIPR will prove capable of quantifying total uteroplacental flow by the early 2nd trimester and fetal flow by late 2nd trimester.

MATERIALS AND METHODS

Animal Population

This study was approved by our institutional animal care and use committee (IACUC). Fifteen healthy, pregnant rhesus macaques received MRI examinations. The gestational ages ranged from late 1st trimester to early 3rd trimester, based on an average term of 166 days in the rhesus macaque [37]. Table 1 gives the gestational age and maternal weight for each rhesus macaque on the first day of imaging. Animals undergoing MRI were pre-medicated with ketamine (10 mg/kg body weight) and general anesthesia was maintained during the course of the procedure with isoflurane gas (1.5% isoflurane/O_2) using an endotracheal tube. Sedation of the pregnant mother resulted in the sedation of the fetus as well. Following imaging, animals were monitored regularly until fully recovered from anesthesia.

MRI Acquisition and Reconstruction

The rhesus macaques were imaged in a right-lateral position on a 3.0 T scanner (Discovery 750, GE Healthcare, Waukesha, WI) with a 32-channel phased array torso coil. The animals were placed in a holder which ensured consistent positioning of the subjects and supported the anterior coil off of their body. 4D flow imaging of the abdomen was performed with a respiratory-gated, radially-undersampled PC VIPR [29,30] acquisition with the following scan parameters: TR/TE=6.1/2.6 ms, FA=8°, VENC=60 cm/s, axial excitation slab length=16 cm, FOV=16×16×16 cm, matrix size=192×192×192, acquired isotropic spatial resolution=0.83 mm; scan duration=10.2 min. Eleven of fifteen rhesus macaques received PC VIPR scans on consecutive days. A subset of five of these monkeys also received two PC VIPR scans on each day of imaging (a total of 13 same-day pairs). The remaining four animals received a single PC VIPR scan on one day, as summarized in Table 1.

Images were reconstructed offline using the signal from an abdominal belt to include only data during expiration (50% efficiency). Reconstructions incorporated corrections for background phase offsets from gradient distortions and concomitant gradients, using polynomial based fitting of background tissue. Time-averaged PC MRAs were created by combining the magnitude and velocity data with complex difference processing [38]. Segmentation of the uteroplacental vessels (UtA/uterine veins (UtV), OSA/ovarian veins (OV)) and fetal vessels (umbilical arteries/vein, fetal aorta, fetal inferior vena cava (IVC)) was performed through signal thresholding and region-growing using MIMICS (Version 17.0, Materialize, Leuven, Belgium). This mask was imported into Ensight (Version 10.0, CEI Inc., Apex, NC) where 2D measurement planes could be manually oriented with respect to a 3D rendering of the segmented vessels, allowing for accurate plane placement in the presence of tortuous vasculature. Time-averaged flow was measured at the uteroplacental vessel midpoints by integrating through-plane velocity components over the segmented vessel areas. Flow measurements in the umbilical vessels were performed at the maternal and fetal ends of the cord (Figure 1), and fetal great vessel measurements were performed proximal to the heart.

Ten of the rhesus macaques imaged on consecutive days received a ferumoxytol injection on the second day of imaging, allowing for the creation of high-resolution, contrast-enhanced angiograms. Ferumoxytol-enhanced angiograms were acquired with a T1-weighted, spoiled gradient echo, 3D ultrashort echo time (UTE) sequence with a center-out radial trajectory [39] before and after an injection of 4 mg/kg ferumoxytol (Feraheme, AMAG Pharmaceuticals, Waltham, WI) diluted 5:1 with saline and infused intravenously over 20 s. The UTE sequence had the following scan parameters: TR/TE=4.4/0.1 ms, FA=10°, FOV=18×18×18 cm^3, matrix size=360×360×360, acquired isotropic spatial resolution=0.5 mm, scan time=5.9 min. Complex subtraction processing was employed to create an angiogram with suppressed background signal. The ferumoxytol-enhanced angiograms were visualized and segmented in MIMICS.

Image Analysis

To assess the relative quality of the PC MRA, the conspicuity of uteroplacental and fetal vasculature was scored in the ferumoxytol-enhanced angiogram and PC MRA for each monkey that received both scans in the same imaging session. Scoring was performed independently by two radiologists (17 and 18 years experience) using the following scale: 1=not visible, 2=partially visible, 3=fully visible. In addition to comparing the scores for each vessel between the two MRA techniques, the impact of gestational age on vessel conspicuity in the PC MRA was examined.

Day-to-day repeatability of PC VIPR measurements was assessed in the 11 monkeys imaged on consecutive days. Same-day repeatability was characterized for the 13 cases where two PC VIPR scans were performed in the same imaging session. Repeatability was assessed by calculating percentage change in flow of the visible uteroplacental vessels between scans. Furthermore, for all animals, inter-observer and intra-observer variability in uteroplacental flow was assessed. Inter-observer variability was assessed by comparing flow measurements from a second observer blinded to the measurement plane placements and results of the

original observer. To assess intra-observer variability, the original observer repeated all uteroplacental flow measurements in each monkey. The observers had 5 and 2 years of experience in 4D flow post-processing, respectively.

Feasibility of using PC VIPR to assess uteroplacental flow was further assessed with a conservation of mass analysis, where in-flow to the uterus was compared against out-flow. When possible, fetal flow consistency was also assessed by measuring percentage change in flow in the fetal IVC to the ascending aorta. Flow consistency in the umbilical cord was assessed by comparing flow in the two umbilical arteries and the umbilical vein at the fetal end and placental ends of the cord.

Statistical Analysis

Continuous variables are reported as mean ± standard deviation. The significance of differences in image scoring between the PC MRA and ferumoxytol-enhanced angiograms for each vessel were compared using a Wilcoxon rank-sum test. Differences in inter-observer scoring for each case were assessed with paired t-tests. Bland-Altman analysis was employed to evaluate the mean difference (d) and 95% limits of agreement (LoA) for same-day and consecutive-day scans, inter-observer variability analysis, and intra-observability variability analysis. Correlation in the repeatability studies was assessed via a linear regression analysis of the repeated flow measurements and calculation of the Pearson correlation coefficient (r). All tests used a threshold of α=0.05 for statistical significance.

RESULTS

Qualitative Assessment

PC VIPR angiograms were successfully reconstructed in all rhesus macaques. Figure 2 shows PC MRAs of representative rhesus macaques in the late 1st trimester, early 2nd trimester, and early 3rd trimester of pregnancy. Radiologist scoring of the MRAs confirmed clear visualization of the UtAs and OVs as early as the end of the 1st trimester, with enhanced visualization of other uteroplacental and fetal vessels by late 2nd trimester. Radiologist scoring (right/left UtA=2.8±0.6/2.9±0.4; right/left OV=2.9±0.2/2.8±0.4) confirmed the UtAs and OVs were fully visible in almost all cases. Notably absent from most segmentations were the UtVs and OSAs, which received lower scores (right/left UtV=1.9±0.2/1.8±0.4; right/left OSA=1.6±0.6/1.5±0.6). These vessels were only fully observed in one rhesus macaque each. The fetal and umbilical vessels were visible in most cases (umbilical/fetal vessels=2.5±0.7/2.5±0.7). A representative segmentation of the fetal and umbilical vessels in the early 3rd trimester of gestation is shown in Figure 3. Figure 4 shows a comparison of segmented PC angiograms in one of the rhesus macaques that received multiple scans on back-to-back days. Angiograms acquired on the same day appeared to be almost identical, while angiograms from back-to-back days showed notable differences in the position of the fetus and the trajectory of the OVs.

High-resolution ferumoxytol-enhanced angiograms were successfully reconstructed in 9 out of 10 rhesus macaques that received contrast. One reconstruction failed due to motion of the mother between the pre- and post-contrast acquisitions. Figure 5 shows a representative

comparison of a ferumoxytol-enhanced angiogram and the corresponding PC angiogram from the same imaging session. Like the PC MRA, the ferumoxytol-enhanced angiograms had excellent visualization of the UtAs and OVs (right/left UtA=2.8±0.4/2.8±0.4; right/left OV=2.9±0.2/2.9±0.2). These angiograms displayed enhanced vessel detail and smaller diameter vessels, allowing for slight improvements in visualization of the UtVs and OSAs (right/left UtV=2.1±0.5/2.2±0.6; right/left OSA=2.1±0.9/1.7±0.5). The average increased visibility in these vessels, however, was not statistically significant. Contrast uptake in the intervillous space allowed for display of the placenta in the reconstructed volume rendering, but fetal and umbilical vasculature was not apparent in any of the ferumoxytol-enhanced angiograms, as expected (umbilical/fetal vessels=1±0/1±0).

Assessment of inter-observer vessel scoring showed excellent agreement in scoring of the UtAs, OVs, and fetal vasculature. Statistically significant differences in scoring were detected for the UtVs and OSAs in the PC MRA and UtVs in the ferumoxytol-enhanced angiograms.

Quantitative Assessment

Since the UtAs and OVs were seen in all rhesus macaques, flow in these vessels was assessed for the same-day and day-to-day repeatability studies. For the same-day repeatability study, both the left and right UtAs were visualized in all scans. The flow measurements in these vessels showed an average relative change of 15% in the left UtA and 11% in the right UtA (d=1.8 mL/min; LoA=−8.5 to 12.0 mL/min; r=0.88). Nineteen of twenty-six measurements showed relative changes less than 15%, with the largest change being 31%. For the day-to-day repeatability measures, 21 of 22 individual UtAs were visualized. These measurements showed an average change in flow between days of 25% in the left UtA and 19% in the right UtA (d=−0.3 mL/min; LoA=−21.5 to 20.8 mL/min; r=0.53). Only 10 of 22 measurements showed changes less than 15%, with the largest relative change being 52%.

The inter-observer and intra-observer repeatability analysis in the UtAs revealed similar measurement distributions to the same-day repeatability analysis. Inter-observer analysis showed an average difference in flow of 16% in the left UtA and 24% in the right UtA (d=0.6 mL/min; LoA=−14.1 to 13.0 mL/min; r=0.75). Intra-observer analysis showed a slightly improved relative difference of 14% in both the right and left UtA (d=0 mL/min; LoA=−12.2 to 12.2 mL/min; r=0.79). Bland-Altman analysis of all four repeatability metrics for the UtAs is presented in Figure 6.

Similar results were observed in the OVs. For the same-day PC VIPR acquisitions, both the left and right OVs were successfully visualized in 11 of 13 scans, with a single vein observed in the other two scans. In these cases, measurements varied an average of 17% in the left OV and 10% in the right OV between scans (d=2.2 mL/min; LoA=−11.9 to 16.4 mL/min; r=0.94). Seventeen of twenty-four venous flow measurements varied less than 15% between scans. For the day-to-day repeatability measurements, both OVs were only apparent in four of the rhesus macaques, with the other seven expressing a single, dominant vein (6 right, 1 left). Flow in the left OV varied an average of 23%, while a similar variation of 24%

was measured in the right OV (d=−2.4 mL/min; LoA=−34.3 to 29.4 mL/min; r=0.80). Only six of fifteen venous flow measurements varied less than 15% between scans.

Inter-observer measurements showed a relative difference of 24% in left OV flow and 12% in the right OV (d=1.6 mL/min; LoA=−24.1 to 27.3 mL/min; r=0.85). Intra-observer measurements were improved with relative differences in flow of 13% in the left OV and 8% in the right OV (d=1.6 mL/min; LoA=−21.0 to 24.3 mL/min; r=0.89). The Bland-Altman analysis of all four repeatability metrics for the OVs is presented in Figure 7.

In the singular cases in which they were fully resolved, flow in the left UtV was measured to be over 20 times less than in the associated UtA and flow in the OSA was approximately 10 times lower than the neighboring OV. Both the UtV and OSA demonstrated cross-sectional areas roughly 25% of their counterparts.

Table 2 gives the time-averaged flow values in each monkey in the UtAs and OVs and the difference in blood flow to and from the uterus and placenta as estimated from these vessels. Although these comparisons were unable to account for smaller flow contributions from the OSAs, UtVs, and other collateral vessels, only an average difference of 15% was observed between placental in-flow and out-flow. Flow in the left and right UtA appeared to be relatively balanced, with similar flow measured in both vessels, while the venous return was more asymmetric, with monkeys displaying a tendency to have a dominant OV. The dominant vein was the right OV in 11/15 monkeys.

With respect to the fetal vasculature, PC VIPR acquisitions typically showed the fetal aorta and IVC by mid-2nd trimester and the full umbilical cord by the end of the 2nd trimester. Flow measurements were possible in the fetal aorta and IVC in 10/15 monkeys, while umbilical flow measurements were acquired in 6/15. The fetal great vessels showed consistency in blood flow, with an average difference in flow between the aorta and IVC of 8%. Reduced consistency was observed in the umbilical vessels, as flow measurements varied on average by 12% in the umbilical arteries and 18% in the umbilical vein between the two ends of the cord.

DISCUSSION

4D flow MRI with PC VIPR was capable of characterizing blood flow to and from the placenta and fetus in one acquisition with good spatial resolution in a clinically feasible scan time. The imaging volume of the PC VIPR acquisition encompassed the maternal descending aorta and IVC, uteroplacental vessels, fetal vessels, uterus, and placenta. This technique proved to be a reliable method of visualizing the UtAs and OVs as soon as late 1st trimester of gestation. On the other hand, the UtVs and OSAs, characterized by smaller diameters and slower flow, could not be fully detected by the early-3rd trimester of gestation, with the exception of one rhesus macaque with a fully resolved left UtV and one with a fully resolved right OSA. In these cases, the low relative flow contributions to the uterus in these vessels were consistent with that reported in the rhesus macaque elsewhere [40]. These results suggest that the primary inflow pathway of blood to the uterus in the rhesus macaque is through the UtAs and the OVs are the primary venous return, rather than blood draining

through the vein corresponding to the artery with which it entered the uterus. This was further reinforced by the close agreement observed in flow measurements into the uterus through the UtAs and from the uterus via the OVs with the consistency analysis. Thus, the absence of the UtVs and OSAs in the PC VIPR images was likely from low flow, and therefore low signal, and vessel diameters the same order as the sequence spatial resolution, resulting in further signal loss from partial volume effects.

The ferumoxytol-enhanced angiograms supported this hypothesis, as the UtVs absent in the PC MRAs were more consistently visible due to enhanced spatial resolution and SNR. These angiograms also allowed consistent visualization of both OVs for all cases, whereas one was sometimes undetected with the PC MRA due to slower flow. Even with improved spatial resolution of this sequence, however, the OSAs were not well-visualized, suggesting they are unlikely to be reliably visualized with PC MRA given their small size in the rhesus macaque. The contrast-enhanced angiograms were not able to characterize fetal vasculature, as measurable amounts of contrast agent did not appear to cross the maternal-fetal interface. Overall, the ferumoxytol-enhanced angiograms proved to be more consistent than the PC angiograms in visualizing small-diameter and slow-flow uteroplacental vessels. Ferumoxytol-enhanced angiograms also proved to be more susceptible to motion artifacts, however, as any motion between the pre- and post-contrast scans would corrupt the image subtraction in the reconstruction. The comparison of these two angiography techniques confirmed that PC VIPR was adequate for visualizing and characterizing the main pathways of placental in-flow and out-flow in the rhesus macaque, as undetected vessels were those with minimal flow contributions.

For the vessel conspicuity scoring, one radiologist had significantly more success in identifying the UtVs and OSAs in both the PC MRA and the ferumoxytol MRA. This can likely be attributed to this observer’s higher experience level in reading uterine MRAs in pregnant subjects and highlights the challenges in detecting these two vessel pairs. While this observer was able to more consistently detect the UtVs and OSAs, their conspicuity was still noticeably lower than in the corresponding arteries and veins.

In both the UtAs and OVs, the repeatability studies showed good correlation and acceptable relative differences in flow measurements from multiple scans acquired on the same day, as well as in inter-observer and intra-observer comparisons. Increased variability was observed between consecutive day scans. The source of the larger disagreement in flow on consecutive days did not appear to be due to technical limitations of PC VIPR, but rather movement of the fetus between scans. For same-day scans, the fetus was sedated for the entirety of the imaging session, preventing significant motion between acquisitions. With scans on back-to-back days, however, the fetus was free to reposition itself in the time between scans. Pressure from the fetus on the placenta and uterine wall could cause blood in the uterine and ovarian vessels to redirect along a path of least resistance, altering blood flow dynamics based on fetal position. This is consistent with the noticeable decrease in measurement correlation between these scans. These results suggested that it may be difficult to discern if longitudinal changes in the flow are from changes in physiology throughout pregnancy or other factors, such as fetal position. A more robust metric would be to assess total UtA flow, rather than flow in the individual UtAs. This measurement would

still be sensitive to physiologic factors such as diurnal flow variations, altered hydration levels, and varying anesthesia exposure between scans, which must be accounted for when designing longitudinal studies.

Improved repeatability was observed in the right-side vessels relative to the left-side, for both same-day and day-to-day comparisons. This was likely a result of the anterior coil being supported off of the rhesus macaque's body. The increased distance of the left-sided vessels to the nearest receiver coil, along with the increased room for respiratory motion on the left side, likely reduced measurement repeatability in these vessels.

While flow through the UtAs was relatively balanced in both the right and left UtAs, this was not the case in the OVs. Each rhesus macaque demonstrated a dominant OV, which carried the majority of blood from the uterus. While 11 of 15 rhesus macaques displayed dominance in their right OV, four monkeys showed a dominant left OV. This suggested the disparity in flow was more than a gravitational effect of the rhesus macaques being imaged in a right-lateral position. We hypothesize that the placentation site influences the flow loads in the two OVs. Unlike humans, who feature a placenta with a single disc, the rhesus macaque has two discs - one of which, the primary disc, is usually larger than the other, the secondary disc. It is possible that while uterine in-flow may initially be distributed relatively equally through the UtAs, some blood may be shunted through the uterine wall to supply the larger placental disc, as there is generally good anastomosis between the two sides. This could contribute to the imbalanced return blood flow.

Quantitative flow assessment of fetal vessels and the umbilical cord proved to be dependent on the gestational age of the fetus. The fetal great vessels were reliably visualized at earlier stages of gestation than the umbilical vessels. The conservation of mass approach conducted in both the great vessels and on opposite ends of the umbilical cord showed good agreement in the great vessels but greater inconsistencies in the umbilical vessels. As with visualizing the UtVs and OSAs, it is likely that spatial resolution was the limiting factor of this application. In the 2nd trimester of gestation, the diameters of the fetal great vessels were typically 5–6 mm, while the umbilical vessels were 3–4 mm. Hence, given their larger diameter, the great vessel flow measurements were less susceptible to partial volume effects, resulting in better agreement than the umbilical vessel measurements and improved visualization earlier in gestation.

We believe this technique represents an improvement over previous attempts to characterize total uteroplacental flow with US and MRI. The ability to retrospectively place measurement planes on data-derived angiograms over a large imaging volume allowed for relatively simple placement of measurement planes orthogonal to the complex, tortuous geometries of many uteroplacental vessels. Dealing with this geometry is a major limitation with US, where challenges with properly aligning acoustic windows with these vessels may result in reduced accuracy. As a result, clinical US examinations do not attempt to image the even more variable venous return, which PC VIPR was able to quantify. In addition, using PC angiograms inherently derived from the data removed the need for a dedicated MRA acquisition, which was cited as the main limitation of previous PC MRI approaches [24,25]. The PC MRA here incorporated all acquired radial projections, which would not be possible

with a Cartesian acquisition because of cardiac pulsatility artifacts. When compared to US, PC VIPR allows for more accurate characterization of flow, as it is directly measured rather than estimated from models. This enhanced accuracy may prove valuable in identifying compromised flow dynamics in high-risk populations, and the ability to reproducibly assess flow as early as late first trimester, as demonstrated here, could aid in early diagnosis. Although PC VIPR was unable to consistently visualize the UtVs and OSAs, these results suggested this was because they were very small and contributed little to total uteroplacental flow. It remains to be seen if the ability to probe flow in these vessels will improve when PC VIPR is scaled up for use in pregnant human subjects, given the increased vessel sizes. Future studies will investigate whether OSAs have larger flow contributions in some subjects, possibly dependent on factors such as placentation site, or if they generally contribute little to total flow.

There were a few limitations with this study. The spatial resolution of the PC VIPR acquisition limited detection of smaller uteroplacental and fetal vasculature. Improvements in spatial resolution would come at the expense of prohibitively long scan times with questionable gains, as even the high-resolution, contrast-enhanced angiograms could not reliably depict the OSAs. The repeatability studies also had relatively small sample sizes and were not designed to completely eliminate outside influences on flow. The same-day acquisitions were not always completed back-to-back in the scanning protocol. Likewise, while scans on consecutive days were attempted to be scheduled at the same time of day, this was not always possible. These gaps between repeatability scans allow the possibility that flow may have been altered due to time-dependent factors such as natural physiologic variations or length of exposure to anesthesia between acquisitions.

The results of this animal study have been encouraging and translation to human studies is currently under investigation. The 4D flow sequence easily scales to the human anatomy and is low in specific absorption rate (SAR). Ferumoxytol, used here for MRA comparisons, is approved for human use as an iron supplement to treat iron deficiencies during pregnancy but not for imaging during pregnancy. In the rhesus model, sedation of the mother eliminated artifacts from gross maternal and fetal body motion and produced more consistent breathing patterns compared to non-sedated imaging in humans. While gating and coaching can be used to limit maternal motion in human subjects, fetal motion cannot be controlled. The radial trajectory of PC VIPR reduces this sequence’s sensitivity to motion [31], but measurements in the moving fetus will be challenging and the impact on image quality and measurement reliability cannot be extrapolated from this study.

In conclusion, 4D flow imaging was feasible in the primary uteroplacental vessels by late 1st trimester and in the fetal vessels by mid-to-late 2nd trimester in the pregnant rhesus macaque. Flow measurements in the uteroplacental and fetal vasculature showed good consistency and repeatability, and comparisons of PC angiograms against higher-resolution, ferumoxytol-enhanced angiograms showed similar depictions of the primary uteroplacental vasculature. These results indicate that 4D flow MRI with PC VIPR could be a valuable tool in assessing uteroplacental health, as it could simultaneously assess blood flow in multiple vessels, which could be further coupled with measurements of placental perfusion, oxygenation, and inflammation from complementary scans.

Acknowledgments

We gratefully acknowledge funding from the NIH and research support from GE Healthcare. We thank AMAG Pharmaceuticals for the donation of ferumoxytol (Feraheme) for this study.

Grant Support: This work was supported by NIH grants U01HD087216 to Dinesh Shah and Oliver Wieben, P51OD011106 to the Wisconsin National Primate Center, and NIH CTSA UW-ICTR UL1TR000427.

References

1. Gagnon R. Placental insufficiency and its consequences. Eur J Obstet Gynecol Reprod Biol. 2003; 110:99–107. DOI: 10.1016/S0301-2115(03)00179-9 [PubMed: 12932881]
2. Lang U, Baker RS, Braems G, Zygmunt M, Künzel W, Clark KE. Uterine blood flow--a determinant of fetal growth. Eur J Obstet Gynecol Reprod Biol. 2003; 110(Suppl):S55–61. DOI: 10.1016/S0301-2115(03)00173-8 [PubMed: 12965091]
3. Bewley S, Cooper D, Campbell S. Doppler investigation of uteroplacental blood flow resistance in the second trimester: a screening study for pre-eclampsia and intrauterine growth retardation. BJOG An Int J Obstet Gynaecol. 1991; 98:871–9. DOI: 10.1111/j.1471-0528.1991.tb13508.x
4. Goldenberg RL, Culhane JF, Iams JD, Romero R. Epidemiology and causes of preterm birth. Lancet. 2008; 371:75–84. DOI: 10.1016/S0140-6736(08)60074-4 [PubMed: 18177778]
5. Habara T, Nakatsuka M, Konishi H, Asagiri K, Noguchi S, Kudo T. Elevated blood flow resistance in uterine arteries of women with unexplained recurrent pregnancy loss. Hum Reprod. 2002; 17:190–4. DOI: 10.1093/HUMREP/17.1.190 [PubMed: 11756386]
6. Guttmacher AE, Maddox YT, Spong CY. The Human Placenta Project: Placental structure, development, and function in real time. Placenta. 2014; 35:303–4. DOI: 10.1016/j.placenta.2014.02.012 [PubMed: 24661567]
7. Schiff E, Mashiach S. The Use of Low Dose Aspirin in Pregnancy. Am J Reprod Immunol. 1992; 28:153–6. [PubMed: 1285867]
8. Cunningham FG, Leveno K, Bloom SL, Spong CY, Dashe JS, Hoffman BL, et al. Williams Obstetrics. 2014
9. Degner K, Magness RR, Shah DM. Establishment of the Human Uteroplacental Circulation: A Historical Perspective. Reprod Sci. 2017; 24:753–61. DOI: 10.1177/1933719116669056 [PubMed: 27733657]
10. Dickey RP. Doppler ultrasound investigation of uterine and ovarian blood flow in infertility and early pregnancy. Hum Reprod Update. 1997; 3:467–503. DOI: 10.1093/humupd/3.5.467 [PubMed: 9528912]
11. Abdallah Y, Naji O, Saso S, Pexsters A, Stalder C, Sur S, et al. Ultrasound assessment of the peri-implantation uterus: A review. Ultrasound Obstet Gynecol. 2012; 39:612–9. DOI: 10.1002/uog.10098 [PubMed: 21910147]
12. Alfirevic Z, Stampalija T, Gyte GML, Neilson JP. Fetal and umbilical Doppler ultrasound in high-risk pregnancies. Cochrane Database Syst Rev. 2009; :1–137. DOI: 10.1002/14651858.CD007529
13. Gudmundsson S, Marsal K. Blood Velocity Waveforms in the Fetal Aorta and Umbilical Artery as Predictors of Fetal Outcome: A Comparison. Am J Perinatol. 1991; 8:1–6. [PubMed: 1987957]
14. Gill R. Measurement of blood flow by ultrasound: accuracy and sources of error. Ultrasound Med Biol. 1985; 11:625–41. [PubMed: 2931884]
15. Kofinas AD, Penry M, Simon NV, Swain M. Interrelationship and clinical significance of increased resistance in the uterine arteries in patients with hypertension or preeclampsia or both. Am J Obstet Gynecol. 1992; 166:601–6. [PubMed: 1536240]
16. Harrington KF, Campbell S, Bewley S, Bower S. Doppler velocimetry studies of the uterine artery in the early prediction of pre-eclampsia and intra-uterine growth retardation. Eur J Obstet Gynecol Reprod Biol. 1991; 42(Suppl):S14–20. [PubMed: 1809604]
17. Newnham JP, Patterson LL, James IR, Diepeveen DA, Reid SE. An evaluation of the efficacy of Doppler flow velocity waveform analysis as a screening test in pregnancy. Am J Obstet Gynecol. 1990; 162:403–10. DOI: 10.1016/0002-9378(90)90396-O [PubMed: 2178428]

18. Sourbron SP, Buckley DL. Tracer kinetic modelling in MRI: estimating perfusion and capillary permeability. Phys Med Biol. 2011; 57:R1–33. DOI: 10.1088/0031-9155/57/2/R1 [PubMed: 22173205]

19. Utz W, Jordan J, Niendorf T, Stoffels M, Luft FC, Dietz R, et al. Blood oxygen level-dependent MRI of tissue oxygenation: Relation to endothelium-dependent and endothelium-independent blood flow changes. Arterioscler Thromb Vasc Biol. 2005; 25:1408–13. DOI: 10.1161/01.ATV.0000170131.13683.d7 [PubMed: 15890970]

20. Israel GM, Malguria N, McCarthy S, Copel J, Weinreb J. MRI vs. ultrasound for suspected appendicitis during pregnancy. J Magn Reson Imaging. 2008; 28:428–33. DOI: 10.1002/jmri.21456 [PubMed: 18666160]

21. Patenaude Y, Pugash D, Lim K, Morin L, Bly S, Butt K, et al. The Use of Magnetic Resonance Imaging in the Obstetric Patient. J Obstet Gynaecol Canada. 2014; 36:349–55. DOI: 10.1016/S1701-2163(15)30612-5

22. Dill T. Contraindications to magnetic resonance imaging. Heart. 2008; 94:943–8. DOI: 10.1136/hrt.2007.125039 [PubMed: 18552230]

23. Gatehouse PD, Keegan J, Crowe LA, Masood S, Mohiaddin RH, Kreitner KF, et al. Applications of phase-contrast flow and velocity imaging in cardiovascular MRI. Eur Radiol. 2005; 15:2172–84. DOI: 10.1007/s00330-005-2829-3 [PubMed: 16003509]

24. Pates JA, Hatab MR, McIntire DD, Cunningham FG, Twickler DM. Determining uterine blood flow in pregnancy with magnetic resonance imaging. Magn Reson Imaging. 2010; 28:507–10. DOI: 10.1016/j.mri.2009.12.009 [PubMed: 20061112]

25. Hawkes RA, Patterson AJ, Priest AN, Harrison G, Hunter S, Pinney J, et al. Uterine artery pulsatility and resistivity indices in pregnancy: Comparison of MRI and Doppler US. Placenta. 2016; 43:35–40. DOI: 10.1016/j.placenta.2016.04.002 [PubMed: 27324097]

26. Dyverfeldt P, Bissell M, Barker AJ, Bolger AF, Carlhäll C-J, Ebbers T, et al. 4D flow cardiovascular magnetic resonance consensus statement. J Cardiovasc Magn Reson. 2015; 17:72.doi: 10.1186/s12968-015-0174-5 [PubMed: 26257141]

27. Francois CJ, Srinivasan S, Schiebler ML, Reeder SB, Niespodzany E, Landgraf BR, et al. 4D cardiovascular magnetic resonance velocity mapping of alterations of right heart flow patterns and main pulmonary artery hemodynamics in tetralogy of Fallot. J Cardiovasc Magn Reson. 2012; 14:16.doi: 10.1186/1532-429X-14-16 [PubMed: 22313680]

28. Ansari SA, Schnell S, Carroll T, Vakil P, Hurley MC, Wu C, et al. Intracranial 4D flow MRI: Toward individualized assessment of arteriovenous malformation hemodynamics and treatment-induced changes. Am J Neuroradiol. 2013; 34:1922–8. DOI: 10.3174/ajnr.A3537 [PubMed: 23639564]

29. Gu T, Korosec FR, Block WF, Fain SB, Turk Q, Lum D, et al. PC VIPR: A high-speed 3D phase-contrast method for flow quantification and high-resolution angiography. Am J Neuroradiol. 2005; 26:743–9. [PubMed: 15814915]

30. Johnson KM, Lum DP, Turski PA, Block WF, Mistretta CA, Ph D, et al. Improved 3D Phase Contrast MRI with Off-resonance Corrected Dual Echo VIPR. Magn Reson Med. 2008; 60:1329–36. DOI: 10.1002/mrm.21763.Improved [PubMed: 19025882]

31. Glover GH, Pauly JM. Projection Reconstruction Techniques for Reduction of Motion Effects in MRI. Magn Reson Med. 1992; 28:275–89. DOI: 10.1002/mrm.1910280209 [PubMed: 1461126]

32. Francois CJ, Srinivasan S, Schiebler ML, Reeder SB, Niespodzany E, Landgraf BR, et al. 4D cardiovascular magnetic resonance velocity mapping of alterations of right heart flow patterns and main pulmonary artery hemodynamics in tetralogy of Fallot. J Cardiovasc Magn Reson. 2012; 14:16.doi: 10.1186/1532-429X-14-16 [PubMed: 22313680]

33. Frydrychowicz A, Landgraf BR, Niespodzany E, Verma RW, Roldán-Alzate A, Johnson KM, et al. Four-dimensional velocity mapping of the hepatic and splanchnic vasculature with radial sampling at 3 Tesla: A feasibility study in portal hypertension. J Magn Reson Imaging. 2011; 34:577–84. DOI: 10.1002/jmri.22712 [PubMed: 21751287]

34. Francois CJ, Lum DP, Johnson KM, Landgraf BR, Bley TA, Reeder SB, et al. Renal Arteries: Isotropic, High-Spatial-Resolution, Unenhanced MR Angiography with Three-dimensional Radial Phase Contrast. Radiology. 2011; 258

35. Dambaeva SV, Durning M, Rozner AE, Golos TG. Immunophenotype and Cytokine Profiles of Rhesus Monkey CD56bright and CD56dim Decidual Natural Killer Cells. Biol Reprod. 2012; 86:1–10. DOI: 10.1095/biolreprod.111.094383

36. Golos TG, Bondarenko GI, Dambaeva SV, Breburda EE, Durning M. On the role of placental major histocompatibility complex and decidual leukocytes in implantation and pregnancy success using non-human primate models. Int J Dev Biol. 2010; 54:431–43. DOI: 10.1387/ijdb.082797tg [PubMed: 19876826]

37. Silk J, Short J, Roberts J, Kusnitz J. Gestation length in rhesus macaques (Macaca mulatta). Int J Primatol. 1993; 14:95–104. DOI: 10.1007/BF02196505

38. Dumoulin C, Souza S, Walker M, Wagle W. Three-Dimensional Phase Contrast Angiography. Magn Reson Med. 1989; 149:139–49.

39. Johnson KM, Fain SB, Schiebler ML, Nagle S. Optimized 3D ultrashort echo time pulmonary MRI. Magn Reson Med. 2013; 70:1241–50. DOI: 10.1002/mrm.24570 [PubMed: 23213020]

40. Wehrenberg W, Chaichareon D, Dierschke D, Rankin J, Ginther O. Vascular Dynamics of the Reproductive Tract in the Female Rhesus Monkey: Relative Contributions of Ovarian and Uterine Arteries. Biol Reprod. 1977; 17:148–53. [PubMed: 406940]

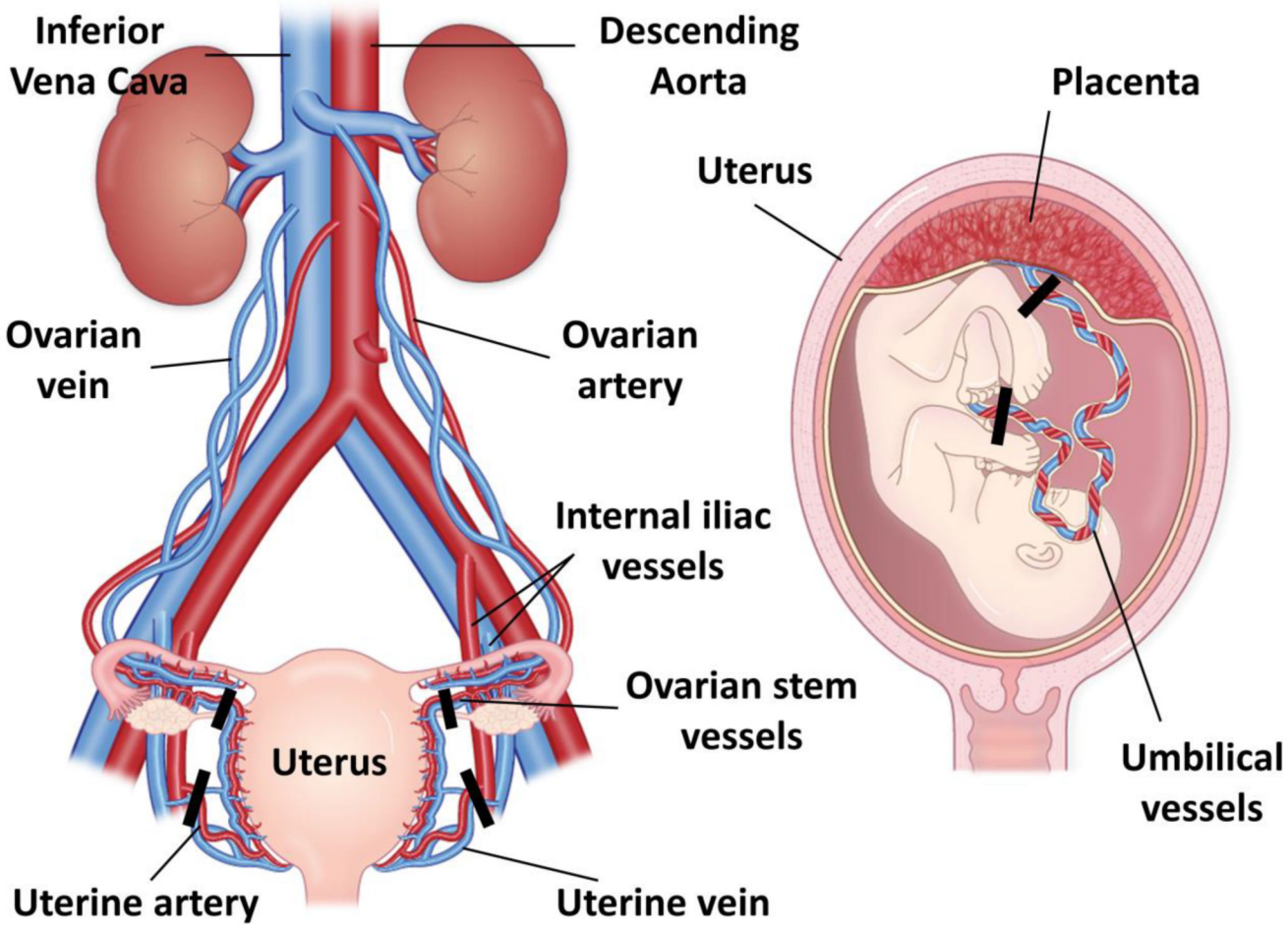

FIGURE 1.

Vascular anatomy of the human placenta. Most of the maternal arterial blood in the placenta is supplied by the uterine arteries with additional contributions from the ovarian stem arteries. Corresponding veins run alongside these vessels. These vessels feed the spiral arteries, which drain into an intervillous space in the placenta where nutrients and oxygen can be transferred to and from the fetal circulation through two umbilical arteries and one umbilical vein in the umbilical cord. Measurement planes of interest to capture total uteroplacental and fetal-placental flow are marked by black bars. Although the rhesus macaque placenta has two distinct discs unlike the single disc in humans, the vascular anatomy is almost identical.

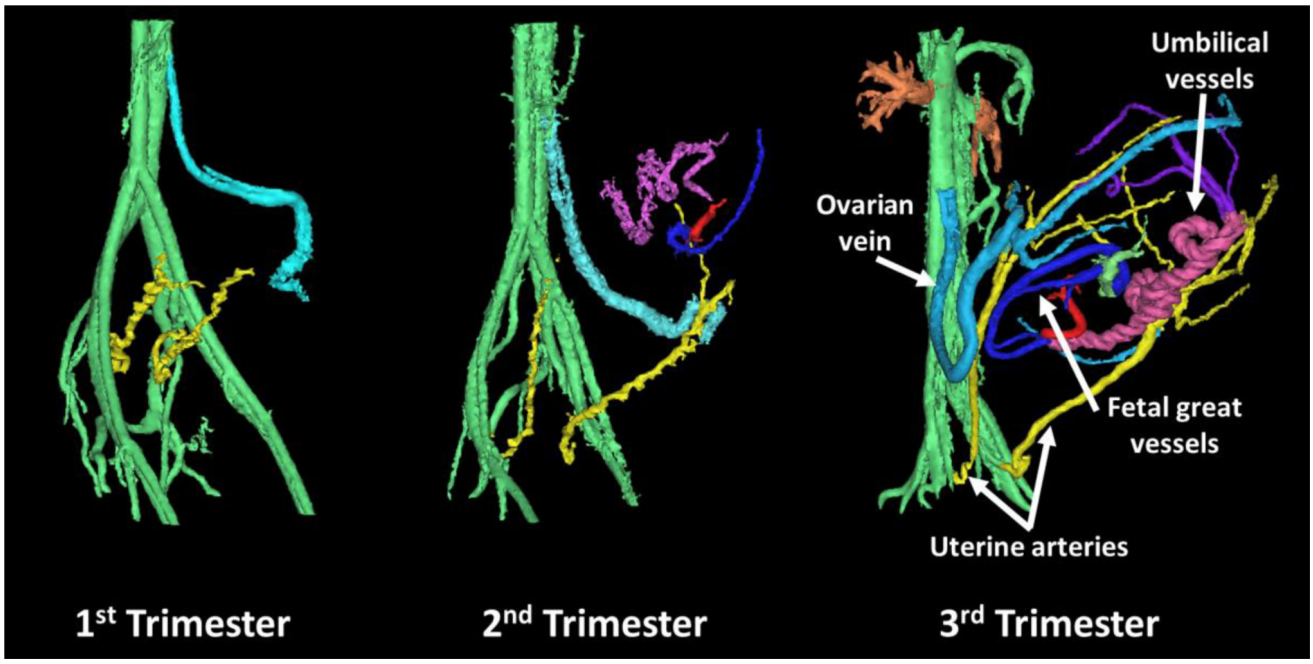

FIGURE 2.

Representative PC MRA of three separate healthy pregnant rhesus macaques at different trimesters of gestation. The main arterial blood supply to the placenta appeared to be the uterine arteries (yellow), while the main venous return was through the ovarian veins (light blue). Uterine veins and ovarian stem arteries were not apparent. While fetal vessels (dark blue and red) were most notable around the 3rd trimester, the main uteroplacental vessels were seen as early as late 1st trimester.

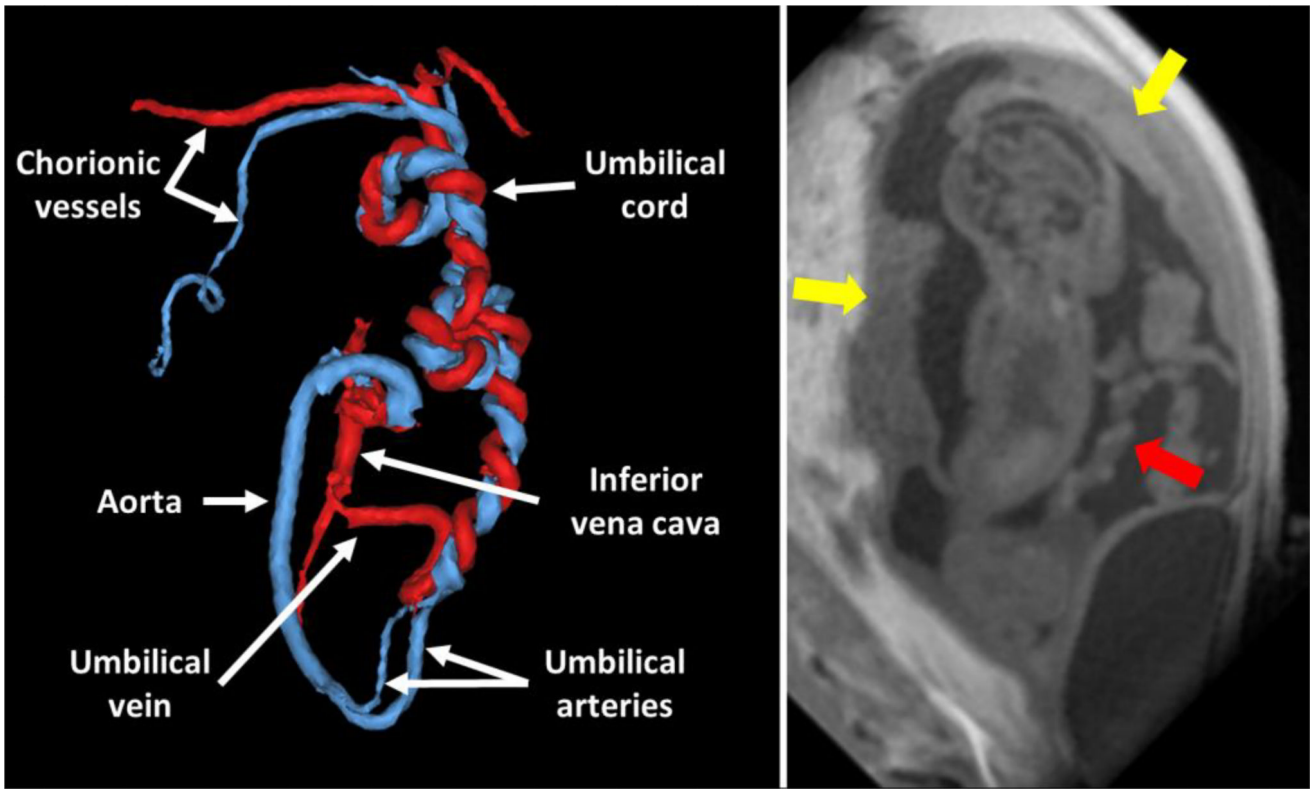

FIGURE 3.

Segmented PC angiogram of the fetal and umbilical vasculature in the early 3rd trimester of pregnancy. The umbilical cord can be seen unbundling into one umbilical vein (red) and two umbilical arteries (blue), one of which forms the aortic arch, in the fetus. A corresponding slice from the PC VIPR magnitude images is shown at the right with the yellow arrows denoting placenta discs and the red arrow showing the umbilical cord.

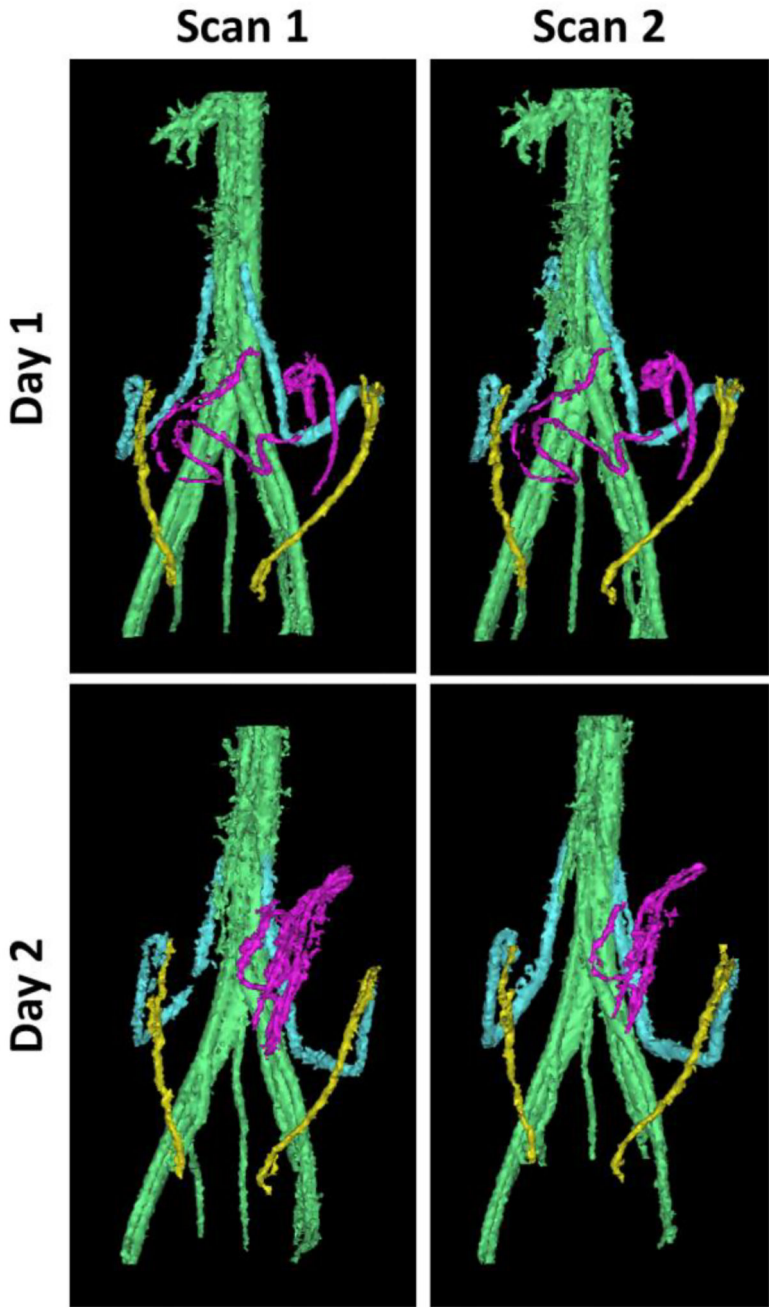

FIGURE 4.

PC angiograms in a single monkey across two days. Two angiograms were acquired on each day. The uterine arteries (yellow) showed minimal motion between days, while the ovarian veins (light blue) and the fetal and umbilical vessels (purple) showed more noticeable changes in position on subsequent days. Same day scans showed similar positioning of all vessels.

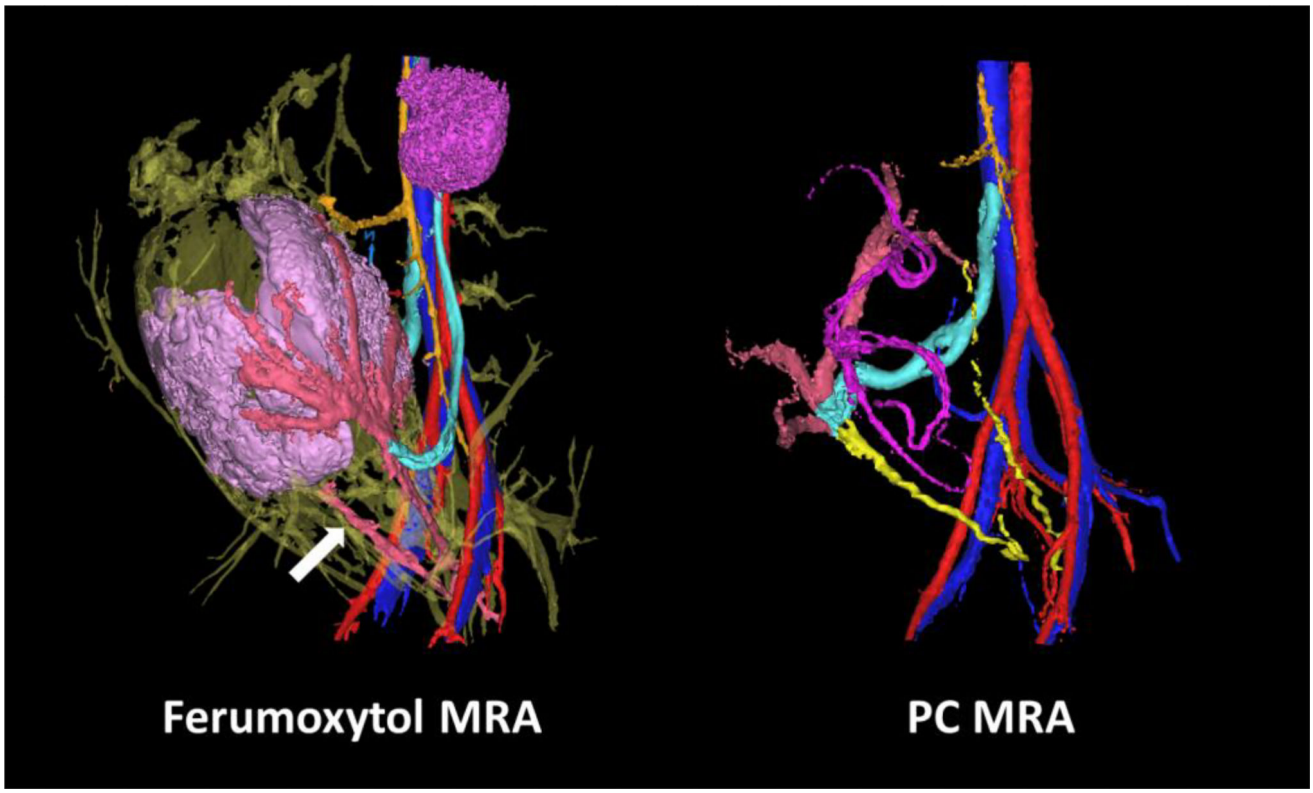

FIGURE 5.

Comparison between ferumoxytol-enhanced angiogram (left) and PC angiogram (right) in the same rhesus macaque on the same day. The color scheme of the uteroplacental and fetal vessels is the same as in Figure 4, except in the ferumoxytol-enhanced angiogram where the uterine arteries and veins, which appear fused together, are a light red (white arrow).

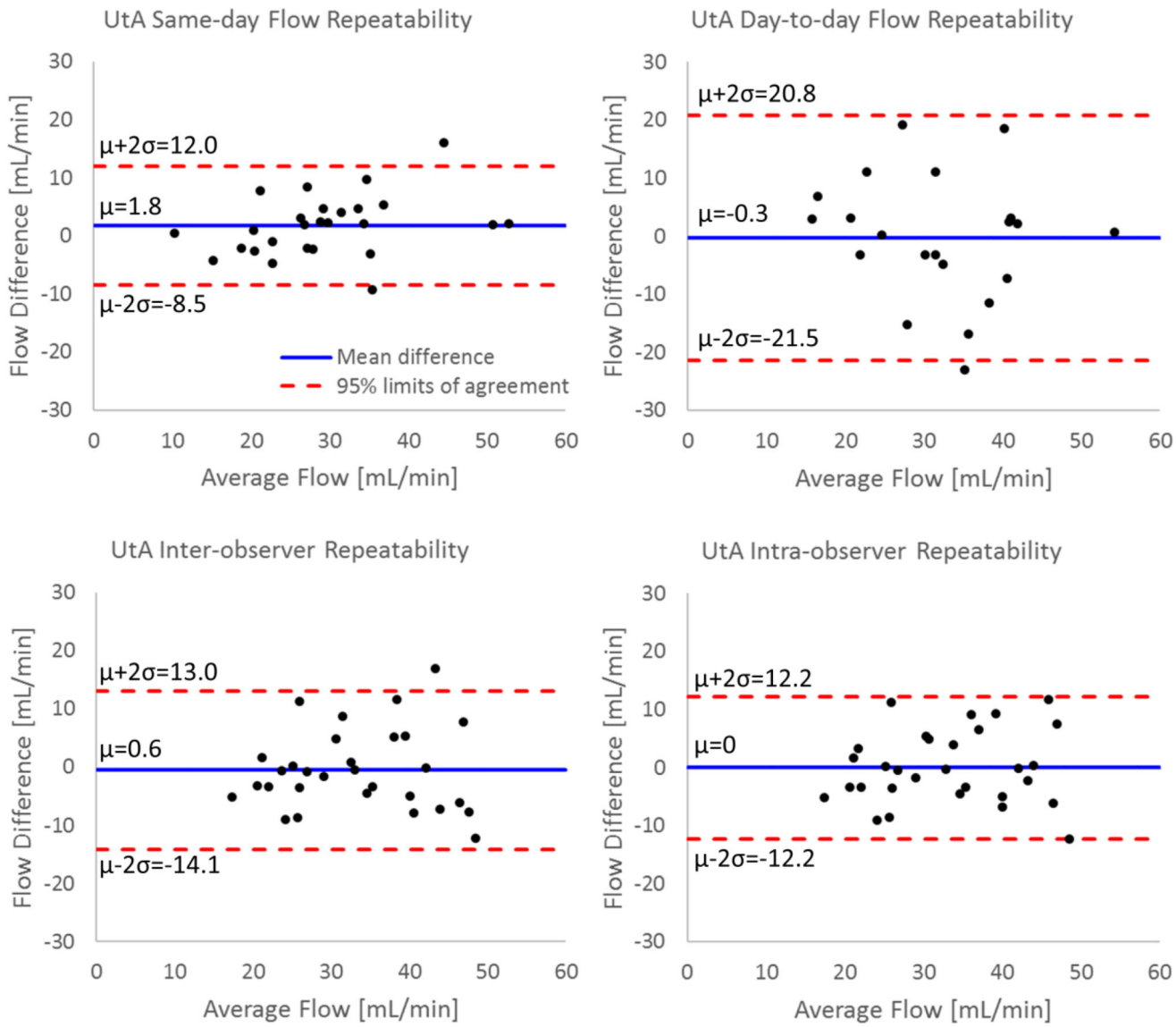

FIGURE 6.

Bland-Altman analysis of flow measurements in the uterine arteries from PC VIPR acquisitions. Repeatability results are presented for repeated scans (test-retest) on the same day and consecutive days, inter-observer analysis, and intra-observer analysis.

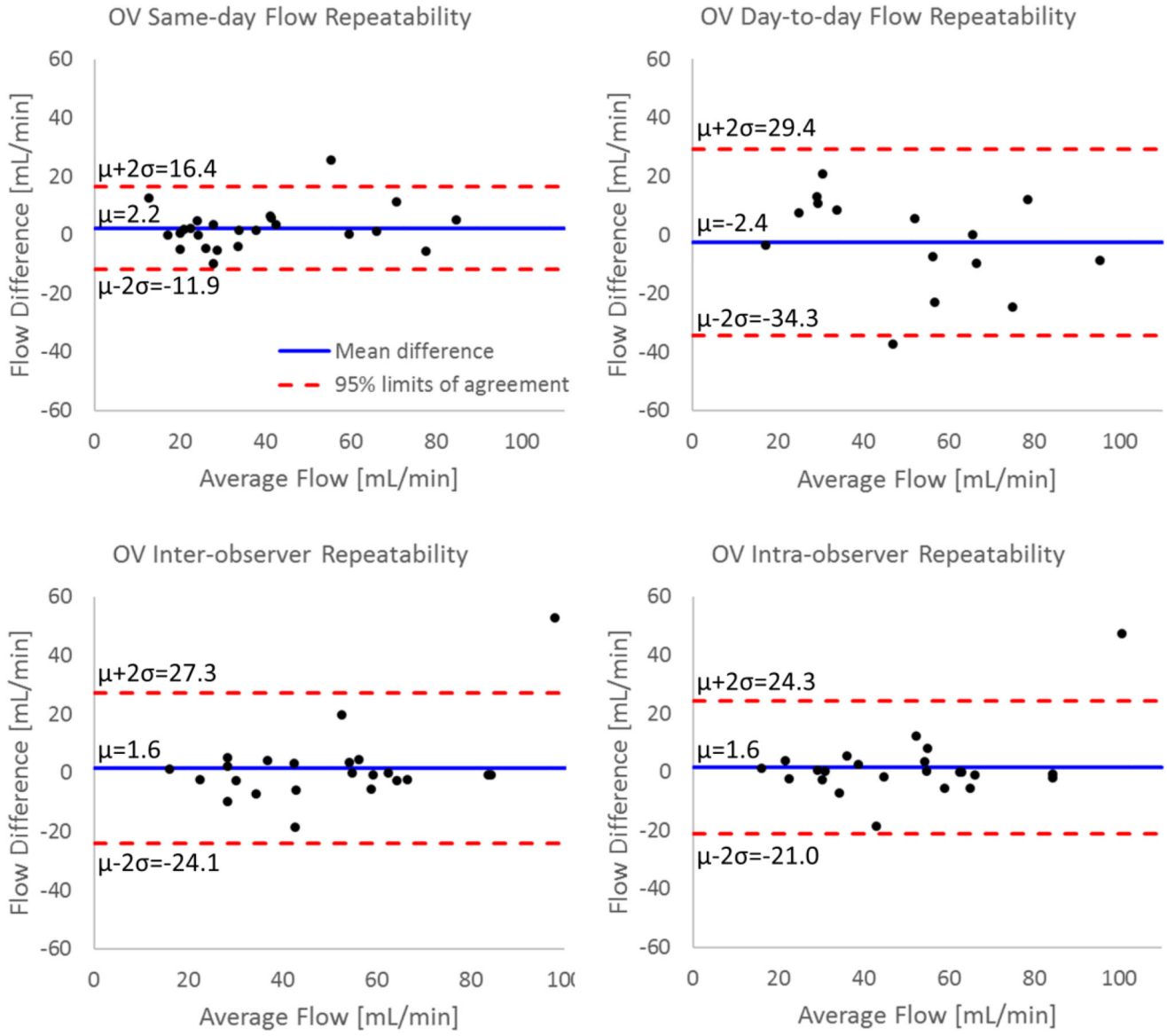

FIGURE 7.

Bland-Altman analysis of flow measurements in the ovarian veins from PC VIPR acquisitions. Repeatability results are presented for repeated scans (test-retest) on the same day and consecutive days, inter-observer analysis, and intra-observer analysis.

Table 1

Gestational ages and maternal weights for imaged rhesus macaque monkeys. The last four columns indicate which MRI scans each monkey received, while the horizontal dashed lines subdivide the rhesus macaques by trimester of gestation.

Rhesus	Weight [kg]	Gestational Age [days][1]	Day-to-day Repeatability	Same-day Repeatability[2]	Single PC VIPR	Ferumoxytol
1	9.70	51	✓	✓✓		
2	8.42	66			✓	
3	8.55	69			✓	
4	9.90	91	✓			✓
5	9.77	92	✓			✓
6	8.56	92	✓			✓
7	8.56	96	✓	✓✓✓		✓
8	7.63	98	✓			✓
9	10.02	98	✓	✓✓		✓
10	9.06	99	✓	✓✓✓		✓
11	7.00	102	✓			✓
12	7.09	103	✓	✓✓✓		✓
13	10.04	106	✓			✓
14	10.58	106			✓	
15	9.97	112			✓	

[1] Average gestational term is the rhesus macaque is 166 days.

[2] Multiple check marks indicate multiple comparisons (on different days) in a monkey.

Table 2

Time-averaged blood flow as measured at the midpoint of the uterine arteries and ovarian veins.

Rhesus	RUtA[1] [mL/min]	LUtA[2] [mL/min]	ROV[3] [mL/min]	LOV[4] [mL/min]	Difference[5]	Change[6] [%]
1	31.5	34.5	66.6	0	−0.6	0.9
2	31.9	33.8	37.6	19.6	8.5	13.0
3	43.4	40.1	76.8	0	6.7	8.0
4	27.5	20.0	50.9	0	−3.4	6.6
5	20.3	29.9	0	54.6	−4.4	8.1
6	33.0	28.2	84.6	0	−23.4	27.7
7	43.2	27.0	61.8	52.2	−43.8	38.4
8	43.8	44.4	28.8	46.2	13.2	15.0
9	22.3	36.9	33.4	30.8	−5.1	7.9
10	23.7	28.6	85.2	0	−32.9	38.6
11	20.3	30.0	63.0	0	−12.7	20.2
12	42.1	49.5	45.7	67.8	−21.8	19.2
13	54.6	37.0	62.6	38.0	−8.9	8.9
14	19.9	42.5	52.6	15.5	−5.6	8.2
15	27.8	25.1	23.8	31.7	−2.6	4.7
Average	**32.4±10.8**	**33.8±8.0**	**51.6±23.9**	**23.8±23.9**	**−9.1±15.6**	**15.0±11.7**

[1] Right uterine artery;

[2] Left uterine artery;

[3] Right ovarian vein;

[4] Left ovarian vein;

[5] Difference = (RUtA+LUtA) - (ROV+LOV);

[6] Change = |Difference / (RUtA+LUtA) * 100|